# High Stability and Luminescence Efficiency in Donor-Acceptor Neutral Radicals Not Following the Aufbau Principle

**Haoqing Guo[1†], Qiming Peng[1, 3†], Xian-Kai Chen[2†], Qinying Gu[4], Shengzhi Dong[1], Emrys W. Evans[4], Alexander J. Gillett[4], Xin Ai[1], Ming Zhang[1], Dan Credgington[4], Veaceslav Coropceanu[2], Richard H. Friend[4*], Jean-Luc Brédas[2*], and Feng Li[1, 4*]**

*[1]State Key Laboratory of Supramolecular Structure and Materials, College of Chemistry, Jilin University, Qianjin Avenue 2699, Changchun, 130012, P. R. China*

*[2]School of Chemistry and Biochemistry and Center for Organic Photonics and Electronics, Georgia Institute of Technology, Atlanta, Georgia 30332-0400, United States*

*[3]Key Laboratory of Flexible Electronics (KLOFE) & Institute of Advanced Materials (IAM), Jiangsu National Synergetic Innovation Center for Advanced Materials (SICAM), Nanjing Tech University (NanjingTech), 30 South Puzhu Road, Nanjing 211816, China.*

*[4]Cavendish Laboratory, University of Cambridge, JJ Thomson Avenue, Cambridge, CB3 0HE, United Kingdom*

*† These authors contributed equally to this work.*

** Authors to whom correspondence should be addressed;*
*E-mail: lifeng01@jlu.edu.cn (FL)； jean-luc.bredas@chemistry.gatech.edu (JLB); rhf10@cam.ac.uk (RHF)*

**With their unusual electronic structures, organic radical molecules display luminescence properties potentially relevant to lighting applications; yet, their luminescence quantum yield and stability lag behind those of other organic emitters. Here, we designed donor-acceptor neutral radicals based on an electron-poor perchlorotriphenylmethyl (PTM) or tris(2,4,6-trichlorophenyl) methyl (TTM) radical moiety combined with different electron-rich groups. Experimental and quantum-chemical studies demonstrate that the molecules do not follow the Aufbau principle: The singly occupied molecular orbital (SOMO) is found to lie below the highest (doubly) occupied molecular orbital (HOMO). These donor-acceptor radicals have a strong emission yield (up to 54%) and high photo-stability, with estimated half-lives reaching up to several months under pulsed UV laser irradiation. Organic light-emitting diodes (OLEDs) based on such a radical emitter show deep-red / near-infrared emission with maximal external quantum efficiency of 5.3 %. Our results provide a simple molecular-design strategy for stable, highly luminescent radicals with non-Aufbau electronic structures.**

Luminescent and stable organic radicals can display unusual electronic structures that are not only of fundamental interest, but can also be exploited in applications such as information storage, fluorescence probes, or chemical sensors.[1-3] Recently, they have been exploited as emitters in organic light-emitting diodes,[4-6] with potential for industrial applications in high-end flat panel displays or light sources. However, to date, while there exist several types of radicals that are sufficiently stable to be isolated and stored under ambient conditions, only very few of them are emissive.[7-11] The development of luminescent radicals thus faces three major challenges: (i) Given the absence of simple molecular-design principles, there are very limited examples of organic luminescent radicals, for example, the perchlorotriphenylmethyl (PTM)[11] and tris(2,4,6-trichlorophenyl)methyl (TTM)[12] radicals, see Figure 1. (ii) The luminescence quantum yields are generally low, on the order of 10% or lower.[13-15] (iii) The photo-stability is poor, for instance, the half-lives for the fluorescence intensities of the PTM and TTM radicals upon ultraviolet irradiation are short (about 100-200 s).[8, 14]

To improve the stability of radical molecules, a common and effective approach is to shield the radical site by using bulky substituents;[16, 17] another strategy is to increase the delocalization of the unpaired electron over a large segment of the backbone.[18, 19] A recent focus of research on organic radicals considered the violation of the Aufbau principle, which was initially introduced by Niels Bohr in 1923 [20] and dictates that 'a maximum of two electrons are put into orbitals in the order of increasing orbital energy'[21]; violating the Aufbau principle of orbital occupation[22-26] has led to tremendously enhanced stability.[26] In the case of radicals with a non-Aufbau electronic structure, the singly occupied molecular orbital (SOMO) lies below the doubly occupied highest occupied molecular orbital (HOMO), namely, there occurs a SOMO-HOMO conversion/inversion (also referred to as a quasi-closed-shell system). However, radicals that violate the Aufbau principle and simultaneously emit light remain very rare.

In the present work, we have designed radical donor-acceptor (D-A$^{\bullet}$) derivatives

based on the electron-poor PTM or TTM radical moiety (A$^{\bullet}$) combined with different electron-rich groups including 9-(naphthalene-2-yl-9H-carbazole (NCz), 1,3-di(9H-carbazol-9-yl)benzene (PDCz), or phenyl-phenothiazine (PPTA) as donor (D), see Figure 1. As we show below, in the D-A$^{\bullet}$ derivatives, the SOMO level (located on the PTM [TTM] radical) lies below the doubly occupied HOMO level (located on the donor fragment); thus, the Aufbau principle is violated. The photo-stability and luminescence quantum yields of these D-A$^{\bullet}$ radicals are both significantly improved with respect to PTM or TTM. Although D-A$^{\bullet}$ luminescent radicals have been reported in earlier investigations,[5, 6, 10] the radical molecules designed here represent the examples where a non-Aufbau behavior is combined with high luminescence efficiency and high stability. Recently, we have shown highly efficient radical-based OLEDs in which the doublet excitons in TTM-3NCz, which follows an Aufbau electronic structure, emit light[6] with electroluminescence internal quantum efficiencies (IQE) approaching 100%. Our present work is also motivated by the quest to further improve the stability of D-A$^{\bullet}$ radical emitters through violation of the Aufbau principle. We find that the maximum external quantum efficiency (EQE) of a solution-processed organic light-emitting diode (OLED) exploiting such a D-A$^{\bullet}$ radical derivative as the emitter reaches up to about 5.3 % (with a deep red / near infrared (NIR) emission peak at about 700 nm), which is among the highest efficiencies for deep red / NIR OLEDs based on purely organic emitters. Our work provides a simple molecular-design strategy for organic non-Aufbau-radical emitters with high luminescence quantum yields and high photostability, and suggests a promising future for non-Aufbau-radical materials for optoelectronic applications.

The molecular structures of the D-A$^{\bullet}$ radicals we synthesized were confirmed by nuclear magnetic resonance (NMR), Fourier transform infrared spectroscopy (FTIR), and matrix-assisted laser desorption/ionization time of flight mass spectrometry (MALDI-TOF-MS), see Section S1 in the Supplementary Information (SI). Their electronic structures were studied by means of electronic paramagnetic resonance (EPR), ultraviolet photoelectron spectroscopy (UPS), cyclic voltammetry (CV)

104 measurements, and quantum-chemical calculations.

105

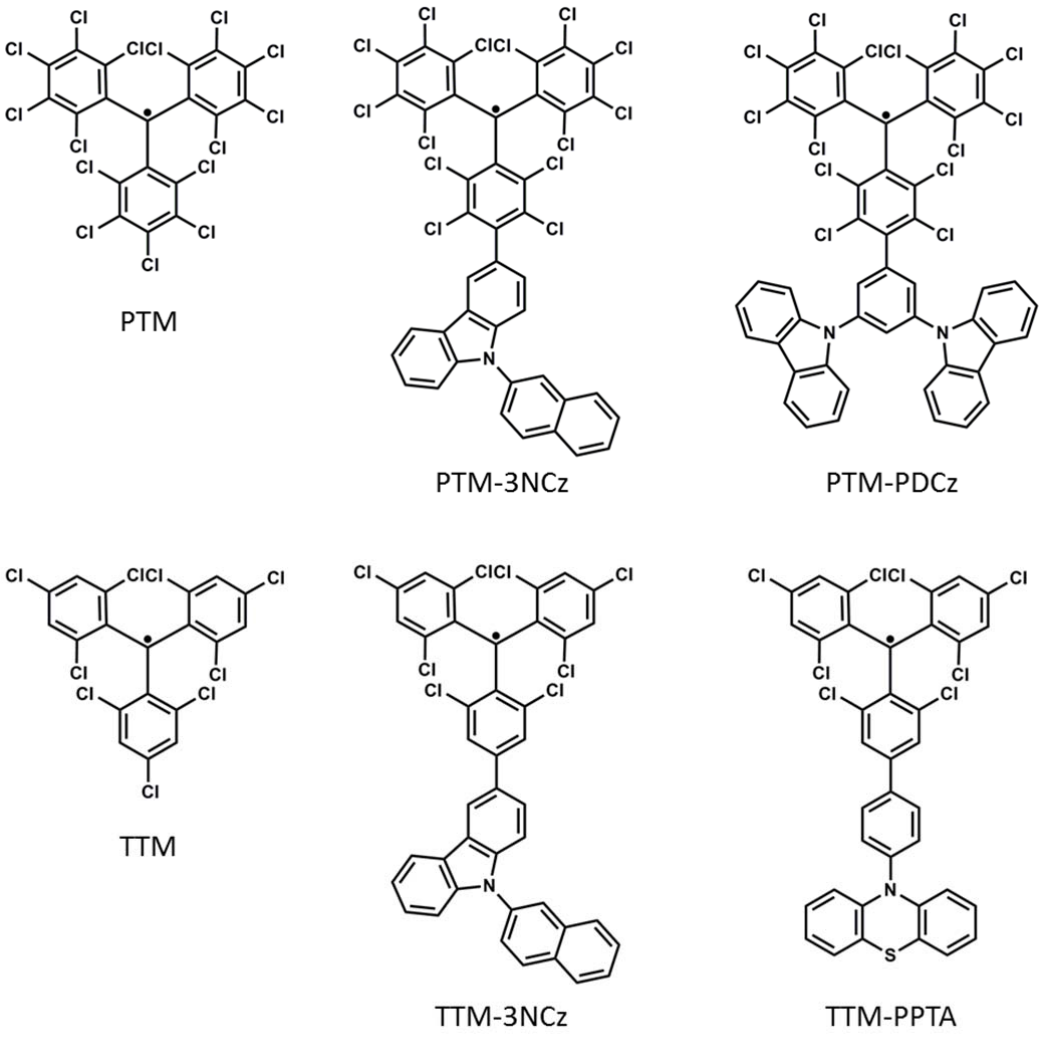


106

107

108 **Fig. 1. Chemical structures of the radical molecules studied here.** Chemical structures of
109 the perchlorotriphenylmethyl (PTM) and tris(2,4,6-trichlorophenyl)methyl (TTM) radicals and of
110 their donor-acceptor radical derivatives with electron-rich groups including
111 9-(naphthalene-2-yl)-9H-carbazole (NCz), 1,3-di(9H-carbazol-9-yl)benzene (PDCz), and
112 phenyl-phenothiazine (PPTA).

113

114 According to the CV measurements (see Table S1 in the SI), in all systems except
115 TTM-3NCz, the oxidation potential of the $A^{\bullet}$ radical is larger than that of the D
116 subunit. If the D-$A^{\bullet}$ electronic structure were to follow the Aufbau principle, this
117 would imply that the electronic ground state correspond to a charge-transfer (CT)

configuration with the unpaired electron (hole) mainly localized on the D fragment. However, the EPR spectra of the D-A$^{\bullet}$ systems (see Figure S1) are very similar to that of the A$^{\bullet}$ radical, indicating that the unpaired electron is localized on the acceptor unit. Quantum-chemical calculations were further performed to assess the electronic structures of the radical derivatives; the computational details are given in the '**Computational methodology**' section. In the isolated PTM radical, the SOMO corresponds as expected to the highest-occupied orbital, see Figure 2a. Interestingly, in PTM-3NCz, the SOMO remains mainly localized on the PTM moiety and lies below the HOMO orbital that is mainly localized on the NCz segment, see Figure 2b; the Aufbau principle is thus clearly violated. Spin density calculations confirm that the unpaired electron in PTM-3NCz is indeed confined to the PTM segment, see Figure 2f. It must be emphasized that the non-Aufbau ground-state electronic configuration calculated for PTM-3NCz at the DFT level is confirmed when using multi-configuration complete-active-space self-consistent field (CASSCF) calculations (see Figure S2). The results of the quantum-chemical calculations also show that the energy ($E_{CT}$) of the CT configuration ($\Psi_{CT}(D^{\bullet+}A^{-})$), which would be expected to be formed according to the Aufbau principle, is significantly larger (> 1 eV) than that of the neutral configuration ($\Psi_{N}(DA^{\bullet})$). As a result, the ground state (GS) of PTM-3NCz is dominated by the neutral electronic configuration with only a small contribution from the CT electronic configuration, namely, $\Psi_{GS}(D\text{-}A^{\bullet}) = \Psi_{N}(DA^{\bullet}) + \alpha\Psi_{CT}(D^{\bullet+}A^{-})$, where the mixing coefficient $\alpha$ is small. Indeed, due to significant intramolecular steric hindrance, there occurs a dihedral angle of about 90° between the carbazole moiety and the perchlorophenyl unit connected to it; in turn, this significantly reduces the electronic coupling between the PTM and NCz segments, leads to negligible hybridization between their orbitals (see Figure 2b), and results in very limited hybridization between the neutral and CT configurations (namely, a small mixing coefficient $\alpha$).

In TTM-3NCz, the oxidation potential of TTM is slightly smaller than that of NCz (see Figure 3a, and Table S1 in the SI). In addition, a much lower dihedral angle of

about 40° between the carbazole unit and the connected dichlorophenyl facilitates the electronic coupling between donor and acceptor fragments. As a consequence, the wavefunctions of the frontier occupied orbitals are delocalized on the TTM and NCz segments (see Figure 2c), with the SOMO located above the doubly occupied HOMO level; thus, the ground-state electronic configuration in TTM-3NCz follows the conventional Aufbau principle. We also note that as a result of the larger electronic coupling, the mixing coefficient $\alpha$ in TTM-3NCz is much larger than in PTM-3NCz; as discussed below, this leads to substantial differences between the absorption spectra of these two systems. Interestingly, when NCz is replaced with the stronger electron-donor PPTA, namely, when, as in the PTM-3NCz case, the oxidation potential of the $A^{\bullet}$ radical is larger than that of the D subunit, a non-Aufbau SOMO-HOMO ordering is reproduced in TTM-PPTA (see Figure 2d). For the same reason, a non-Aufbau orbital ordering is also observed in PTM-PDCz (see Figure 2e).

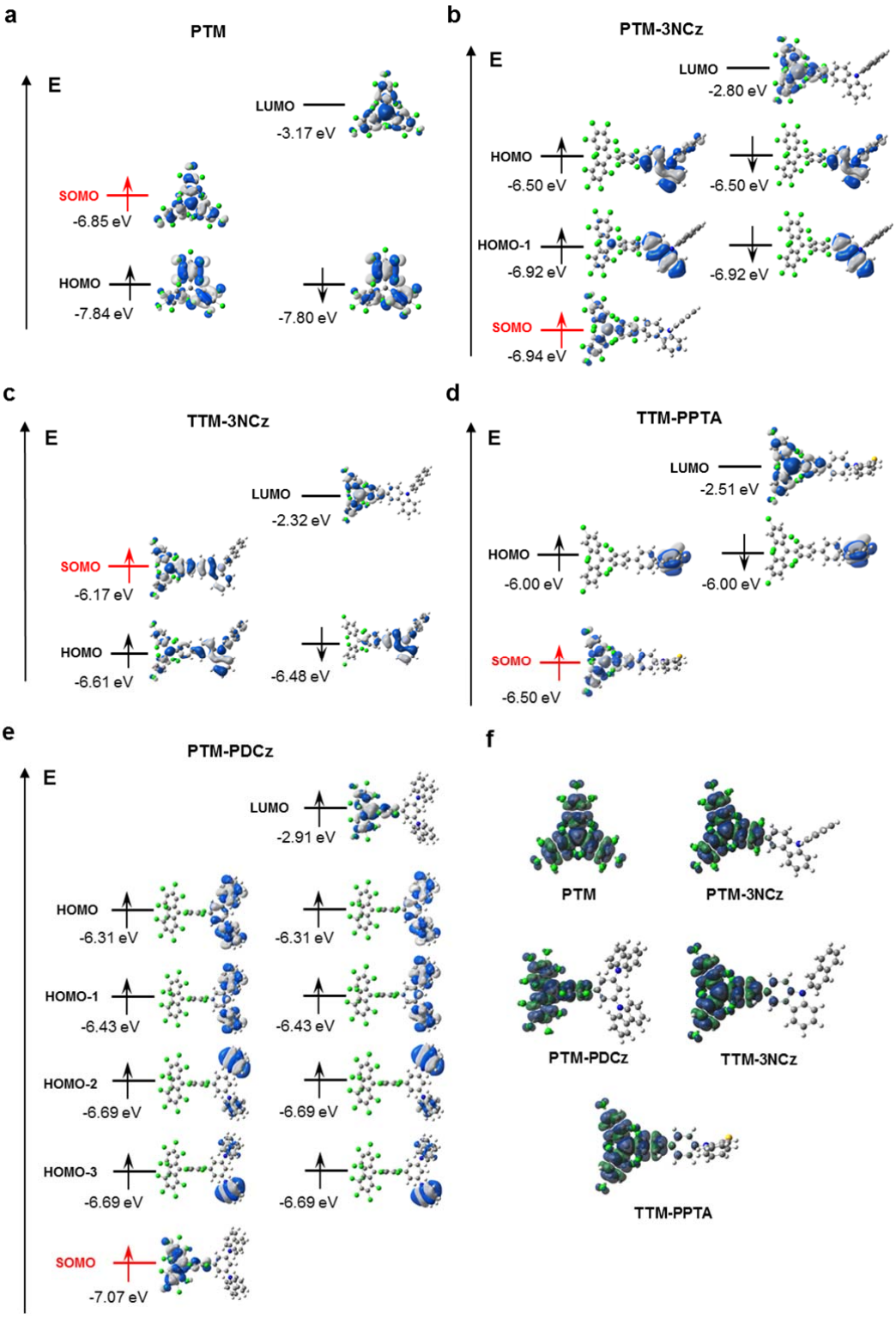


**Fig. 2. Quantum-chemical results for the PTM, PTM-3NCz, TTM-3NCz, TTM-PPTA, and PTM-PDCz radicals.** Energies and wavefunctions for the frontier molecular orbitals of the: **a)**

PTM, **b**) PTM-3NCz, **c**) TTM-3NCz, **d**) TTM-PPTA, and **e**) PTM-PDCz radicals, as calculated at the tuned ωB97XD/6-31+G(d,p) level of theory. **f)** Calculated spin density in the PTM, PTM-3NCz, TTM-3NCz, TTM-PPTA, and PTM-PDCz radicals. The two colors used for the electron wavefunctions distinguish the wavefunction phases; the white, gray, blue, and green spheres in the chemical structures represent H, C, N, and Cl atoms, respectively.

The violation of the Aufbau principle in the designed D-A$^{\bullet}$ radicals is also supported by CV and UPS data. Figure 3a and Table S1 present the redox characteristics of the A$^{\bullet}$ radicals (such as PTM or TTM), the isolated D molecules (such as NCz or PPTA), the D-A$^{\bullet}$ radicals (such as PTM-3NCz, TTM-3NCz, or TTM-PPTA), and their hydrogenated precursors D-HA (see Scheme S2 in the SI). For HPTM-3NCz, only one oxidation peak is observed at +1.26 V, which is in line with the +1.17 value in NCz. For PTM-3NCz, an oxidation peak similar to that in HPTM-3NCz appears at +1.24 V. In addition, another oxidation peak as well as a new reduction potential feature appear at +1.60 V and -0.58 V, respectively; these features are not observed in HPTM-3NCz. Importantly, the oxidation potential at +1.60 V and the reduction potential at -0.58 V for PTM-3NCz are in excellent agreement with the redox characteristics of the PTM radical (oxidation potential at +1.57 V and reduction potential at -0.46 V), as shown in Figure 3a and Table S1. Thus, the cyclic voltammetry data are also fully consistent with the peculiar non-Aufbau electronic structure of the PTM-3NCz radical and with the DFT results that show only weak hybridization between PTM and NCz orbitals. We also note that since the HOMO-1 energy is very close to that of the SOMO (by 0.02 eV according to the DFT calculations), the oxidation potential at +1.60 V could have contributions from both these levels. Similar CV results are found in TTM-PPTA and PTM-PDCz (see Figure 3a). On the contrary, in TTM-3NCz, the oxidation potential (+1.08 V) of TTM is slightly smaller than that (+1.17 V) of NCz, leading to a conventional Aufbau electronic structure. Interestingly, the +0.71 V oxidation potential of TTM-3NCz is significantly smaller than those measured for TTM (+1.08 V) and NCz (+1.17 V), indicating a significant hybridization between the TTM and NCz orbitals and thus a larger contribution (a larger mixing coefficient $\alpha$) of the CT configuration to the

ground state in TTM-3NCz than in PTM-3NCz, which is fully consistent with the DFT results.

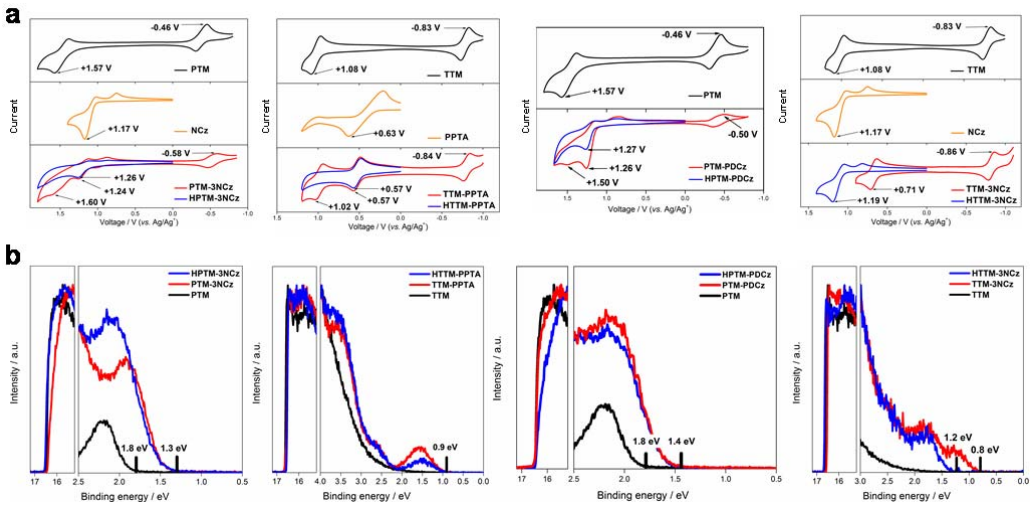


**Fig. 3. Experimental data for the PTM, TTM, PTM-3NCz, TTM-PPTA PTM-PDCz, and TTM-3NCz radicals. a,** Cyclic voltammetry characteristics. **b,** Ultraviolet photoelectron spectra of the thin films: Left: Normalized cutoff side of the UPS spectra; right: Enlarged low binding-energy side.

Figure 3b shows the UPS spectra of the thin films. For PTM, PTM-3NCz, and HPTM-3NCz, the low binding-energy sides of the UPS spectra are markedly different. The onset in PTM is located at around 1.8 eV below the Fermi energy ($E_F$ = 4.7 eV), implying a first ionization energy ($IE_1$) of 6.5 eV, which is assigned to the SOMO orbital (to be compared with our calculated value of about -6.9 eV for an isolated radical molecule). The onset in the closed-shell HPTM-3NCz molecule appears at ~ 1.3 eV below $E_F$, corresponding to an $IE_1$ value of ~ 6.0 eV; this is assigned to its HOMO, which is consistent with our calculated value of -6.5 eV for the NCz-localized HOMO. In the PTM-3NCz radical, the valence band onset coincides with that of HPTM-3NCz (rather than that of the PTM radical). This implies that the $IE_1$ values of the PTM-3NCz radical and the closed-shell HPTM-3NCz molecular system are very close, which fully agrees with the results of our calculations and CV

measurements, showing that their HOMO energies are nearly equal. Importantly, the UPS data indicate that the highest occupied level in the PTM-3NCz radical is *not* the PTM SOMO, but a doubly occupied level on the NCz group and, thus, confirm the non-Aufbau behavior. Similar UPS characteristics are also found in the TTM-PPTA and PTM-PDCz radicals (see Figure 3b). We also note that, in contrast to PTM, the intensity of the UPS onset for TTM is very weak and no clear peak related to the SOMO is observed. As a result, the UPS spectra of TTM-PPTA and HTTM-PPTA are very similar over a larger energy range in comparison to the systems based on PTM. Overall, the results of the quantum-chemical calculations and the UPS and CV measurements establish a clear picture of the violation of the Aufbau principle in PTM-3NCz, TTM-PPTA, and PTM-PDCz. In contrast to the D-A$^{\bullet}$ radicals discussed above, the valence band onset in the UPS spectrum of TTM-3NCz is located at a lower binding energy than that of HTTM-3NCz. This implies that the electronic structure of TTM-3NCz follows the Aufbau principle, which is attributed to the significant hybridization between the TTM and NCz orbitals, as obtained in the DFT results.

We now turn to the photophysical properties of the radicals investigated here, see Figure 4 and Table 1. The optical absorption spectra of the PTM and PTM-3NCz radicals show an absorption maximum at ~ 380 nm, with an additional feature in PTM-3NCz at 607 nm. The quantum-chemical results allow us to assign the former to a local π-π* excitation on the PTM radical segment while the latter corresponds to a typical CT excitation, see the calculated Natural Transition Orbitals (NTOs)[27] in Figure 4a. In addition, we note that a similar low-energy absorption at about 566 nm is also found in PTM, which according to our calculations arises from an electronic transition involving orbitals localized on the PTM central carbon and on one of the tetrachlorophenyl groups. Moreover, the fluorescence spectrum of PTM-3NCz shows a significant red-shift compared to that of PTM, as well as strong solvatochromic effects that are not observed in the pristine PTM radical (Figure S6 in the SI). The intensity of the CT band is proportional to the mixing coefficient α. Therefore, a much

weaker CT transition observed experimentally (see Figure 4b) and a smaller oscillator strength ($f$ = ~ 0.0095) estimated by our DFT calculations in PTM-3NCz are additional evidence of a smaller hybridization between the CT and neutral electronic configurations, compared to TTM-3NCz [6] ($f$ = ~ 0.123).

Interestingly, in all the D-A$^{\bullet}$ systems, the reduction potential (electron affinity) of the D-A$^{\bullet}$ system is comparable to that of the A$^{\bullet}$ fragment. This can be explained by the fact that after forming an anionic configuration ($A^-$), the CT transition involving the SOMO of PTM or TTM can no longer occur, which contributes to suppress the overall hybridization between donor and acceptor orbitals. This switching-off of the donor-acceptor electronic coupling also rationalizes why: (i) the HOMO energy of the D-HA hydrogenated precursors is nearly equal to that of the D fragments; and (ii) the low-energy transitions are not observed in the D-HA molecules.

We also performed transient absorption (TA) and PL measurements on PTM-3NCz, as shown in Figure S11. The photo-induced absorptions (PIA) at around 600-700 nm and 1550-1650 nm are ascribed to characteristic absorptions of $NCz^+$ and $PTM^-$, respectively.[28] The overlap of the decay curves of PL and PIA of $NCz^+$ and $PTM^-$ together with the results of steady-state spectra in solvents with different polarities, indicate that the lowest excited doublet state ($D_1$) in PTM-3NCz has a CT character, as shown in Figure 4a. Thus, the TA measurements also establish that the CT configuration in PTM-3NCz has a higher energy than the neutral configuration for which the unpaired electron lies on PTM; this supports our rationalization of why PTM-3NCz has a non-Aufbau ground-state electronic configuration. The photo-physics data obtained for TTM-PPTA also point to $D_1$ being a CT state (see Figures S7 and S12 in the SI). Similar photophysical characteristics were also found in other D-A$^{\bullet}$ radicals reported earlier.[9]

The fluorescence quantum yield ($\Phi_f$) of the PTM-3NCz radical in cyclohexane is very high, about 54.0% and 52.0% upon excitation at 380 nm and 607 nm, respectively (Table 1). Since no significant difference is observed for these two excitation wavelengths, it can be concluded that Kasha's rule remains obeyed. These

values are over 30 times higher than that of PTM ($\Phi_f$ = 1.6 %, excited at 377 nm). The radiative and non-radiative decay rates ($k_r$ and $k_{nr}$) of the radicals were obtained from the results of fluorescence quantum yield and lifetime (Figure S8), see Table 1. Interestingly, the $k_{nr}$ of the PTM-3NCz radical is ten times lower than that of PTM. Such low $k_{nr}$ values were also reported in other D-A$^{\bullet}$ radicals.[9] It is useful to note that the non-radiative transition (internal conversion) rates from $D_1$ to $D_0$ depend on the square of their vibronic (non-adiabatic) couplings.[29] Since these couplings are proportional to the spatial overlap between the $D_1$ and $D_0$ wavefunctions (see Section S11 in the SI),[29-30] the CT-excitation character of the $D_1$ state is expected to reduce the non-adiabatic couplings and thus the $D_1 \rightarrow D_0$ internal conversion rates, as has been shown in the case of thermally activated delayed fluorescence (TADF) emitters.[31-32] Following earlier work,[29, 33] we have estimated the non-adiabatic couplings between the $D_1$ and $D_0$ states for PTM and PTM-3NCz, see Figure 4c. The results indeed indicate that the $D_1$-$D_0$ non-adiabatic couplings in PTM-3NCz are much smaller than those in PTM, which is in line with the experimental data.

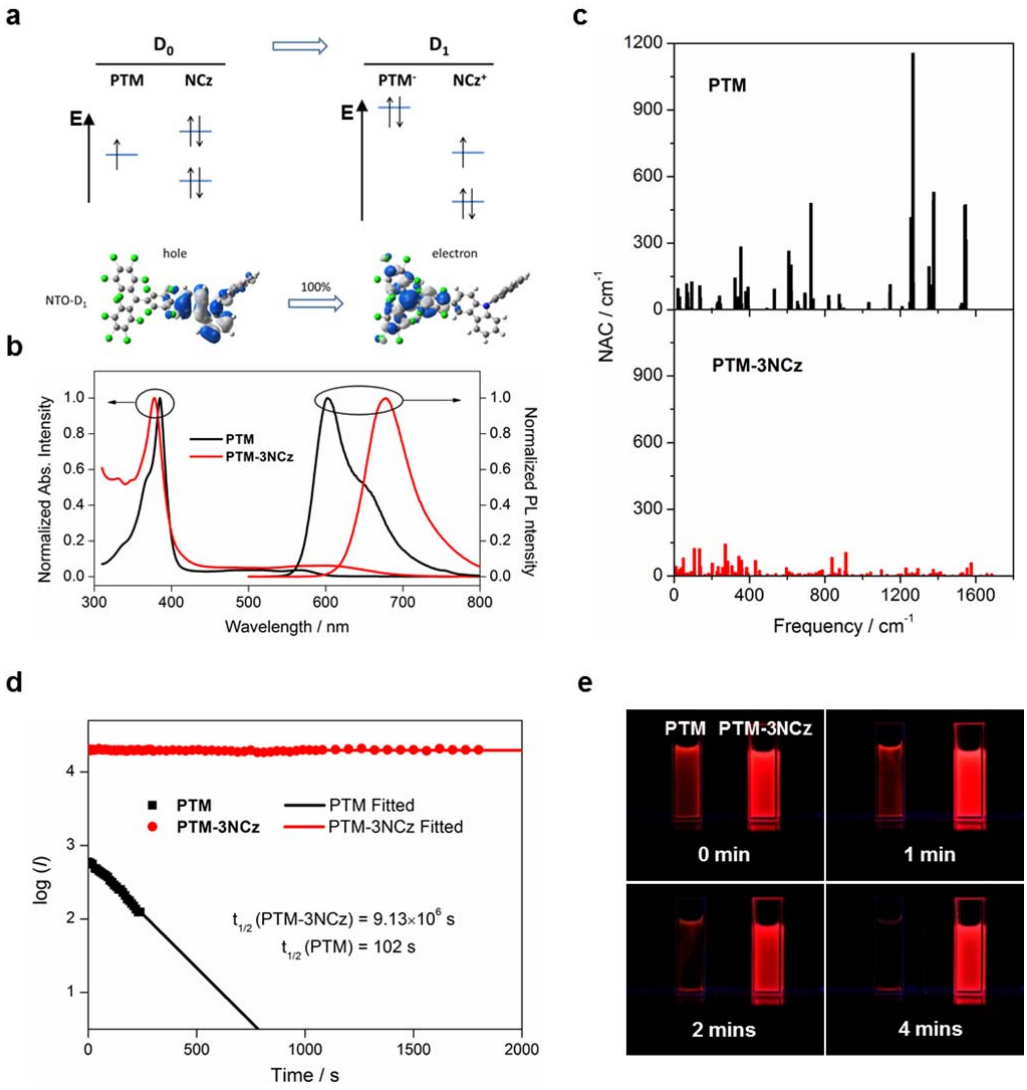


**Fig. 4. Photo-physical properties and photo-stability of the PTM-3NCz radical. a,** Schematics of the electronic transition process between the ground state ($D_0$) and the first excited state ($D_1$) in PTM-3NCz. The two colors used for the electron wavefunctions distinguish the wavefunction phases; the white, gray, blue, and green spheres in the chemical structures represent H, C, N, and Cl atoms, respectively. **b,** Optical absorption and fluorescence spectra of the PTM and PTM-3NCz radicals in cyclohexane. **c**, Calculated non-adiabatic couplings (NAC) between the first excited state ($D_1$) and the ground state ($D_0$) in the PTM and PTM-3NCz radicals. **d**, Time dependence of the emission intensities (I) of the PTM and PTM-3NCz radicals in dilute cyclohexane under 355 nm laser radiation. **e**, Photographs of PTM and PTM-3NCz in dilute cyclohexane solution under 365 nm UV lamp as a function of time.

**Table 1**. Photophysical parameters (at 300 K) of the PTM and PTM-3NCz radicals in cyclohexane.

| | $\lambda_{abs}$[a] (nm) | $\lambda_f$[b] (nm) | $\Phi_f$ / $\lambda_{ex}$[c] (%) / (nm) | $\tau_f$[d] (ns) | $k_r$[e] ($\times10^6$ $s^{-1}$) | $k_{nr}$[e] ($\times10^6$ $s^{-1}$) |
|---|---|---|---|---|---|---|
| PTM | 377, 566 | 605 | 1.6 / 377 | 5.4 | 2.9 | 182.3 |
| PTM-3NCz | 380, 607 | 680 | 54.0 / 380<br>52.0 / 607 | 26.3 | 20.5 | 17.5 |

[a] Peaks of ultraviolet-visible absorption. [b] Wavelength of the maximum fluorescence emission. [c] Fluorescence quantum yield and corresponding excitation wavelength. [d] Fluorescence lifetime. [e] Radiative and non-radiative decay rates calculated by using the maximum fluorescence quantum yield and corresponding lifetime data.

We now assess the photo-stability of the D-A$^{\bullet}$ radicals, which is an important element in the development of luminescent paramagnetic molecular-based materials.[1, 34] Here, all the radicals were exposed to a pulsed laser radiation at 355 nm. In the case of the PTM radical, the emission is unstable and the fluorescence intensity decays rapidly, with a fitted half-life ($\tau_{1/2}$) of only 102 s, see Figure 4d. On the contrary, the half-life of fluorescence intensity for PTM-3NCz greatly increases to $9.13\times10^6$ s, a value nearly 5 orders of magnitude higher than that of PTM and 2-4 orders of magnitude higher than those of other derivatives reported in the literature.[6, 12-14] We suggest that the origin of this remarkable stability improvement is two-fold: (i) Due to the non-Aufbau behavior of the D-A$^{\bullet}$ radicals, the SOMO electrons can be shielded by the outer HOMO electrons. (ii) Compared to the local character of the $\pi$-$\pi^*$ excited states of the PTM radical, the charge-transfer nature of the $D_1$ excited states can make the photocyclization reactions in the D-A$^{\bullet}$ radicals more difficult. We note that, in addition to the PTM-3NCz radical, enhanced fluorescence quantum yield and improved photo-stability are also observed in other D-A$^{\bullet}$ radicals, such as PTM-PDCz, PTM-PCz, PTM-3PCz, and TTM-PPTA (see Table S2 and Figure S10).

Due to the carbon–chlorine bond cleavage issue, we were unable to use these radical emitters to fabricate OLEDs via vacuum thermal evaporation. Thus, OLED devices based on the PTM-3NCz emitter were solution processed and fabricated by means of spin coating (see the '**Device fabrication and measurement'** section), as shown in Figure 5a. The devices display deep red / NIR emission with an

electroluminescence (EL) peak at about 700 nm (see inset of Figure 5c). The maximum external quantum efficiency (EQE) of the optimized device is about 5.3 %, which ranks among the highest EQE values for deep red / NIR OLED devices exploiting purely organic emitters [35,36] (see Table S3). Figures 5b and 5c show the current density–voltage and radiance–voltage profiles of this device and the evolution of the EQE value versus current density, respectively. The EL spectra from 10.5 V to 15 V are shown in Figure S13a; there appears no significant change as the voltage increases across this range, which confirms that the device emission comes from PTM-3NCz. The data for five other solution-processed OLED devices are given in Figure S13b. A more detailed discussion of the radical-based OLEDs is given in Section S15.

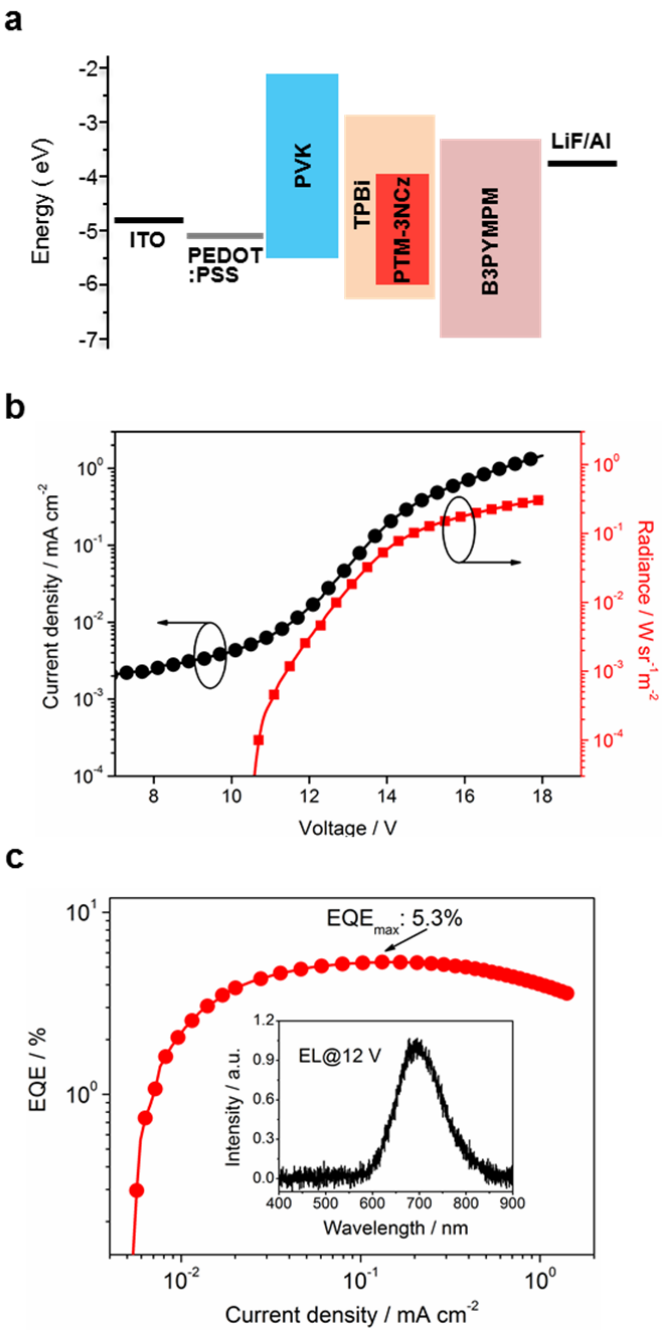


**Fig. 5. Optoelectronic properties of the OLED device with PTM-3NCz as the emitter. a,** Schematic diagram of the structure of the PTM-3NCz-based OLED. **b,** Current density–voltage (black circles) and radiance–voltage (red squares) profiles. **c,** External quantum efficiency (EQE) of the OLED as a function of current density; the inset shows the full EL spectrum at 12 V.

In summary, we have designed donor-acceptor neutral radicals based on the electron-poor PTM or TTM radical group combined with different electron-rich groups. Due to the strong electron-withdrawing ability of the PTM [TTM] radical, the energy of the singly occupied level (localized on PTM [TTM]) is lower than that of the HOMO level coming from the donor group. This results in the violation of the Aufbau principle, confirmed by the results of quantum-chemical calculations as well as optical absorption, ultraviolet photoelectron spectroscopy (UPS), and cyclic voltammetry (CV) data. The non-Aufbau behavior of these D-A$^{\bullet}$ radicals leads to excellent photostability (for example, half-lives of up to several months of their fluorescence intensities). The fluorescence quantum yields are high (up to 54%), due to significantly reduced non-radiative transition rates. In addition, OLEDs exploiting one of the D-A$^{\bullet}$ radical derivative as emitter shows deep red / NIR emission at 700 nm, with a maximum EQE as high as 5.3 %.

Overall, our work provides a simple molecular-design strategy for organic luminescent radicals that do not follow the Aufbau principle and demonstrate simultaneously high luminescent quantum yields and high photostability. It also paves the pathway toward high-efficiency OLEDs exploiting purely organic non-Aufbau-radical molecules with deep red or NIR emission.

**Data availability.** The data that support the results of this study are available from the corresponding authors upon reasonable request.

**Acknowledgements**

H. Guo, Q. Peng, S. Dong, X. Ai, M. Zhang, and F. Li are grateful for financial support from the National Natural Science Foundation of China (Grant No. 91833304, 51673080, 11804156), National Key R&D Program of China (Grant No. 2016YFB0401001), National Key Basic Research and Development Program of China (973 program, Grant No. 2015CB655003), and Program of "JLUSTIRT" (Grant No. 2019TD-33). Q. Peng acknowledges support from the Nanjing Tech

Start-up Grant (38274017104). X.-K. Chen, V. Coropceanu, and J.L. Bredas acknowledge support from the Georgia Institute of Technology, Georgia Research Alliance, Vasser-Woolley Foundation, and Kyulux. Q. Gu, D. Credgington, E. W. Evans, A. J. Gillett and R. H. Friend would like to thank the EPSRC for funding this work (EP/M01083X/1, EP/M005143/1). Q. Gu is also grateful for financial support from China Scholarship Council (CSC) and Cambridge Trust. D. Credgington also acknowledges support from the Royal Society (grant no. UF130278). F. Li is an academic visitor at the Cavendish Laboratory, Cambridge, and is supported by the Talents Cultivation Program (Jilin University, China).

## Author Contributions

H. Guo, Q. Peng, S. Dong, X. Ai, M. Zhang performed the synthesis and experimental measurements under the supervision of F. Li. X.-K. Chen carried out the quantum-chemical calculations under the supervision of J.L. Bredas, and V. Coropceanu participated in the discussion of the theoretical calculations. E. Evans participated in the discussion of the photophysics mechanism, and A. J. Gillett conducted the transient absorption measurements under the supervision of R. H. Friend. Qinying Gu performed the device fabrications and measurements under the supervision of Dan Credgington. All authors discussed the results and contributed to writing the manuscript.

## Additional information

**Competing interests:**The authors declare no competing interests.

**Supporting Information** accompanies this paper at http://www.nature.com/

## References


1. Simao, C.; Mas-Torrent, M.; Crivillers, N.; Lloveras, V.; Manuel Artes, J.; Gorostiza, P.; Veciana, J.; Rovira, C., A Robust Molecular Platform for Non-Volatile Memory Devices with Optical and Magnetic Responses. *Nature Chemistry* **2011**, *3*, 359-364.
2. Morita, Y., et al., Thermochromism in an Organic Crystal Based on the Coexistence of Sigma- and Pi-Dimers. *Nature Materials* **2008**, *7*, 48-51.
3. Dhimitruka, I.; Bobko, A. A.; Eubank, T. D.; Komarov, D. A.; Khramtsov, V. V., Phosphonated Trityl Probes for Concurrent in Vivo Tissue Oxygen and Ph Monitoring Using Electron Paramagnetic Resonance-Based Techniques. *Journal of the American Chemical Society* **2013**, *135*, 5904-5910.
4. Peng, Q.; Obolda, A.; Zhang, M.; Li, F., Organic Light-Emitting Diodes Using a Neutral Π Radical as Emitter: The Emission from a Doublet. *Angewandte Chemie International Edition* **2015**, *54*, 7091-7095.
5. Obolda, A.; Ai, X.; Zhang, M.; Li, F., Up to 100% Formation Ratio of Doublet Exciton in Deep-Red Organic Light-Emitting Diodes Based on Neutral Π-Radical. *ACS Applied Materials & Interfaces* **2016**, *8*, 35472-35478.
6. Ai, X; Evans, E. W.; Dong, S.; Gillett, A. J.; Guo, H.; Chen, Y.; Hele, T. J. H.; Friend, R. H.; Li, F., Efficient radical-based light-emitting diodes with doublet emission. *Nature* **2018**, 563, 536-540.
7. Hattori, Y.; Kusamoto, T.; Nishihara, H., Enhanced Luminescent Properties of an Open-Shell (3,5-Dichloro-4-Pyridyl)Bis(2,4,6-Trichlorophenyl)Methyl Radical by Coordination to Gold. *Angewandte Chemie International Edition* **2015**, *54*, 3731-3734.
8. Hattori, Y.; Kusamoto, T.; Nishihara, H., Luminescence, Stability, and Proton Response of an Open-Shell (3,5-Dichloro-4-Pyridyl)Bis(2,4,6-Trichlorophenyl)Methyl Radical. *Angewandte Chemie International edition* **2014**, *53*, 11845-8.
9. Heckmann, A.; Dummler, S.; Pauli, J.; Margraf, M.; Kohler, J.; Stich, D.; Lambert, C.; Fischer, I.; Resch-Genger, U., Highly Fluorescent Open-Shell Nir Dyes: The Time-Dependence of Back Electron Transfer in Triarylamine-Perchlorotriphenylmethyl Radicals. *The Journal of Physical Chemistry C* 2**009**, *113*, 20958-20966.
10. Velasco, D.; Castellanos, S.; Lopez, M.; Lopez-Calahorra, F.; Brillas, E.; Julia, L., Red Organic Light-Emitting Radical Adducts of Carbazole and Tris(2,4,6-Trichlorotriphenyl)Methyl Radical That Exhibit High Thermal Stability and Electrochemical Amphotericity. *Journal of Organic Chemistry* **2007**, *72*, 7523-7532.
11. Fox, M. A.; Gaillard, E.; Chen, C. C., Photochemistry of Stable Free Radicals: The Photolysis of Perchlorotriphenylmethyl Radicals. *Journal of the American Chemical Society* **1987**, *109*, 7088-7094.
12. Armet, O.; Veciana, J.; Rovira, C.; Riera, J.; Castaner, J.; Molins, E.; Rius, J.; Miravitlles, C.; Olivella, S.; Brichfeus, J., Inert Carbon Free Radicals. 8. Polychlorotriphenylmethyl Radicals: Synthesis, Structure, and Spin-Density Distribution. *The Journal of Physical Chemistry* **1987**, *91*, 5608-5616.
13. Ai, X.; Chen, Y.; Feng, Y.; Li, F., A Stable Room-Temperature Luminescent Biphenylmethyl Radical.

*Angewandte Chemie International Edition* **2018**, *57*, 2869-2873.

14. Hattori, Y.; Kusamoto, T.; Nishihara, H., Highly Photostable Luminescent Open-Shell (3,5-Dihalo-4-Pyridyl)Bis(2,4,6-Trichlorophenyl)Methyl Radicals: Significant Effects of Halogen Atoms on Their Photophysical and Photochemical Properties. *RSC Advances* **2015**, *5*, 64802-64805.

15. Kimura, S.; Tanushi, A.; Kusamoto, T.; Kochi, S.; Sato, T.; Nishihara, H., A Luminescent Organic Radical with Two Pyridyl Groups: High Photostability and Dual Stimuli-Responsive Properties, with Theoretical Analyses of Photophysical Processes. *Chemical Science* **2018**, *9*, 1996-2007.

16. Hicks, R. G., What's New in Stable Radical Chemistry? *Organic & Biomolecular Chemistry* **2007**, *5*, 1321-1338.

17. Ballester, M.; Riera-Figueras, J.; Castaner, J.; Badfa, C.; Monso, J. M., Inert Carbon Free Radicals. I. Perchlorodiphenylmethyl and Perchlorotriphenylmethyl Radical Series. *Journal of the American Chemical Society* **1971**, *93*, 2215-2225.

18. Schweyen, P.; Brandhorst, K.; Wicht, R.; Wolfram, B.; Broring, M., The Corrole Radical. *Angewandte Chemie International Edition* **2015**, 54, 8213-8216.

19. Sun, Z.; Ye, Q.; Chi, C.; Wu, J., Low Band Gap Polycyclic Hydrocarbons: From Closed-Shell near Infrared Dyes and Semiconductors to Open-Shell Radicals. *Chemical Society Reviews* **2012**, *41*, 7857-7889.

20. Bohr, N., Über die Anwendung der Quantentheorie auf den Atombali[1]). I. Die Grundpostulate der Quantentheorie. *Zeitschrift für Physik* **1923**, *13*, 117-165.

21. Mallion, R. B.; Rouvray, D. H., Molecular Topology and the Aufbau Principle. *Molecular Physics* **1978**, *36*, 125-128.

22. Wang, Y.; Zhang, H.; Pink, M.; Olankitwanit, A.; Rajca, S.; Rajca, A., Radical Cation and Neutral Radical of Aza-Thia [7] Helicene with Somo− Homo Energy Level Inversion. *Journal of the American Chemical Society* **2016**, *138*, 7298-7304.

23. Gryn'ova, G.; Coote, M. L.; Corminboeuf, C., Theory and Practice of Uncommon Molecular Electronic Configurations. *Wiley Interdisciplinary Reviews: Computational Molecular Science* **2015**, *5*, 440-459.

24. Franchi, P.; Mezzina, E.; Lucarini, M., Somo–Homo Conversion in Distonic Radical Anions: An Experimental Test in Solution by Epr Radical Equilibration Technique. *Journal of the American Chemical Society* **2014**, *136*, 1250-1252.

25. Kusamoto, T.; Kume, S.; Nishihara, H., Cyclization of Tempo Radicals Bound to Metalladithiolene Induced by Somo-Homo Energy-Level Conversion. *Angewandte Chemie-International Edition* **2010**, *49*, 529-531.

26. Gryn'ova, G.; Marshall, D. L.; Blanksby, S. J.; Coote, M. L., Switching Radical Stability by Ph-Induced Orbital Conversion. *Nature Chemistry* **2013**, *5*, 474-481.

27. Martin, R. L., Natural Transition Orbitals. *The Journal of Chemical Physics* **2003**, *118*, 4775-4777.

28. Komamine, S.; Fujitsuka, M.; Ito, O.; Itaya, A., Photoinduced electron transfer between C60 and

carbazole dimer compounds in a polar solvent. *Journal of Photochemistry and Photobiology A: Chemistry* **2000**, *135*, 111–117.

29. Niu, Y.; Peng, Q.; Deng, C.; Gao, X.; Shuai, Z., Theory of Excited State Decays and Optical Spectra: Application to Polyatomic Molecules. *The Journal of Physical Chemistry A* **2010**, *114*, 7817-7831.

30. Hayashi, M.; Mebel, A. M.; Liang, K. K.; Lin, S. H., Ab Initio Calculations of Radiationless Transitions between Excited and Ground Singlet Electronic States of Ethylene. *The Journal of Chemical Physics* **1998**, *108*, 2044-2055.

31. Shizu, K.; Uejima, M.; Nomura, H.; Sato, T.; Tanaka, K.; Kaji, H.; Adachi, C., Enhanced Electroluminescence from a Thermally Activated Delayed-Fluorescence Emitter by Suppressing Nonradiative Decay. *Physical Review Applied* **2015**, *3*, 014001-014007.

32. Shizu, K.; Noda, H.; Tanaka, H.; Taneda, M.; Uejima, M.; Sato, T.; Tanaka, K.; Kaji, H.; Adachi, C., Highly Efficient Blue Electroluminescence Using Delayed-Fluorescence Emitters with Large Overlap Density between Luminescent and Ground States. *The Journal of Physical Chemistry C* **2015**, *119*, 26283-26289.

33. Chen, X.-K.; Ravva, M. K.; Li, H.; Ryno, S. M.; Brédas, J.-L, Effect of Molecular Packing and Charge Delocalization on the Nonradiative Recombination of Charge-Transfer States in Organic Solar Cells. *Advanced Energy Materials* **2016**, *6*, 1601325.

34. Sugawara, T.; Komatsu, H.; Suzuki, K., Interplay between Magnetism and Conductivity Derived from Spin-Polarized Donor Radicals. *Chemical Society Reviews* **2011**, *40*, 3105-3118.

35. Kim, D.-H.; D'Aléo, A.; Chen, X.-K.; Sandanayaka, A. D. S.; Yao, D.; Zhao, L.; Komino, T.; Zaborova, E.; Canard, G.; Tsuchiya, Y.; Choi, E.; Wu, J. W.; Fages, F.; Brédas, J.-L.; Ribierre, J.-C.; Adachi, C. High-efficiency electroluminescence and amplified spontaneous emission from a thermally activated delayed fluorescent near-infrared emitter. *Nature Photonics* **2018**, *12*, 98-104.

36. Ye, H.; Kim, D. H.; Chen, X.; Sandanayaka, A. S. D.; Kim, J. U.; Zaborova, E.; Canard, G.; Tsuchiya, Y.; Choi, E. Y.; Wu, J. W.; Fages, F.; Bredas, J.-L.; D'Aléo, A.; Ribierre, J.-C.; Adachi, C., Near-Infrared Electroluminescence and Low Threshold Amplified Spontaneous Emission above 800 nm from a Thermally Activated Delayed Fluorescent Emitter. *Chemistry of Materials* **2018**, *30*, 6702-6710.

## Methods

### Materials synthesis and characterization

All chemicals and reagents for syntheses and measurements were purchased from commercial suppliers and used without further purification, unless otherwise stated. Tetrahydrofuran and chloroform were redistilled before use. The $^{1}$H-NMR spectra were recorded at 298 K with a Bruker AVANCZ 500 spectrometer, using deuterated

dimethyl sulfoxide as solvent and tetramethylsilane as standard. Mass spectra were measured on a Thermo Fisher ITQ1100 GC-MS mass detector. FTIR spectra were tested by VERTEX 80V.

**Electronic paramagnetic resonance (EPR) measurements**

The electronic paramagnetic resonance spectra of the powder samples were measured using a JES-FA200 EPR spectrometer at ambient temperature.

**Ultraviolet photoelectron spectroscopy (UPS)**

Thin films (20 nm) were fabricated via spin-coating onto clean ITO-coated glass substrates. The UPS spectra were measured on a VG scienta XPS/UPS System under ultrahigh vacuum ($10^{-8}$ Pa). A monochromatized He Iα irradiation from discharged lamp supplies photons with 21.22 eV for UPS.

**Cyclic voltammetry**

The cyclic voltammetry (CV) measurements were performed using an electrochemical analyzer (CHI660E, CH Instruments, USA). A glass carbon disk was used as the working electrode. A platinum wire acted as the counter electrode and Ag/Ag+ acted as the reference electrode together with the redox couple ferrocenium/ferrocene as the internal standard at the rate of 100 $mV \cdot s^{-1}$. Tetrabutylammonium hexafluorophosphate in anhydrous dimethyl formamide and anhydrous dichloromethane (0.1 M) were used as the supporting electrolyte for the negative and positive scans, respectively.

**Spectral measurements**

For the UV-vis absorption and fluorescence measurements, the radicals were dissolved into solvents at a concentration of $1 \times 10^{-5}$ $molL^{-1}$. The UV-vis spectra were measured using a Shimadzu UV/Vis spectrophotometer (UV-2550). The fluorescence spectra of the samples excited at around 380 nm were recorded by a Shimadzu spectrofluorophotometer (RF-5301PC).

**Lifetime measurements**

An Edinburgh fluorescence spectrometer (FLS980) was used, the lifetime of the excited states was measured by the time-correlated single-photon-counting method

(detected at the peak of the PLs) under 378.8 nm laser excitation with a pulse width of 68.9 ps.

**Transient absorption (TA) measurements (PTM-3NCz and TTM-PPTA)**

Sample photoexcitation in the transient absorption (TA) experiments was achieved by the second and third harmonics (532 and 355 nm) of an electronically triggered Q-switched Nd:YVO4 (1 ns pump length, Advanced Optical Technologies Ltd AOT-YVO-25QSPX): fluence = 97.8 μJ/cm$^2$ @532 nm for PTM-3NCz and 6.0 μJ/cm$^2$ @355 nm for TTM-PPTA. The probe was generated by home-built broadband non-collinear optical parametric amplifiers (NOPAs), pumped using the 800 nm fundamental output of a commercially available Ti:sapphire amplifier (Spectra Physics Solstice Ace) for the probe in the 1200 – 1675 nm region and the frequency-doubled output (400 nm) for probes in the 520 – 1150 nm regions . The delay between probe and pump pulses was varied using a Stanford DG645 delay generator. The transmitted probe pulses were collected with a silicon dual-line array detector which was driven and read out by a custom-built board from Stresing Entwicklungsbüro.

**Photo-stability measurements**

The radicals were dissolved into cyclohexane with a concentration of $5\times10^{-5}$ mol L$^{-1}$. The solutions in quartz cells were bubbled with nitrogen and then sealed, for eliminate the influence of oxygen. A Nd:YAG (yttriumaluminum-garnet) laser working at 355 nm (pulse width: 10 ns, frequence: 10 Hz ) with a power intensity of 21.4 kw/cm$^2$, was used to irradiate the samples. The emission spectra were detected using a Maya 2000 Pro fiber spectrometer.

**Computational methodology**

The initial geometries of the closed-shell precursors of the radicals were optimized by employing the range-separated ωB97XD functional (with the default range-separation parameter ω of 0.2 bohr$^{-1}$) and the 6-31+G(d,p) basis set.[37] Following our previous investigations,[35,38] an iteration procedure was employed to non-empirically tune the ω parameters with the implicit consideration of the dielectric environment via the

polarizable continuum model (PCM; solvent: cyclohexane). Then, ωB97XD/6-31+G(d,p) with optimal ω parameters was employed to optimize the ground-state geometries of the radicals and calculate the vibrational frequencies. Time-dependent density functional theory (TD-DFT) was employed to study the excited-state properties; all the excited-state properties of these radicals were examined at the TD ωB97XD/6-31+G(d,p) level with optimal ω parameters. To confirm the relevance of the electronic configurations obtained at the DFT ωB97XD level, we have taken the PTM and PTM-3NCz molecules as examples and calculated their ground-state electronic structures with the CASSCF approach. All the quantum-chemical calculations were performed with the Gaussian 09 Rev D01 program.[39]

**Device fabrication and measurement**

Indium tin-oxide (ITO; WF ~ 4.8 eV) coated glass substrates were used and subsequently cleaned by sonication in acetone and 2-propanol for 10 minutes, followed by $O_2$ plasma treatment for 10 minutes. PEDOT: PSS (Clevios CH4083, LumTech Taiwan) was spin-casted on top of the ITO under ambient conditions and annealed on a hot plate at 160°C for 20 minutes, forming a 40 nm-thick film. The PEDOT: PSS-coated substrates were then transferred to a nitrogen-filled glovebox to conduct the following solution processes. Poly(9-vinylcarbazone) (PVK, Sigma-Aldrich) was spin-casted onto the PEDOT: PSS layer at the concentration of 15mg/ml in toluene (Sigma-Aldrich) followed with an annealing process for 30 min at 150°C. The annealed films were spin-rinsed with chlorobenzene (Sigma-Aldrich) to remove the residual soluble material and baked at 90°C for 10 min to remove the remaining rinsing solvent and form a compact interlayer with the thickness of around 10 nm. The 50 nm-thick emitting layer (EML) of TPBi (LumTech Taiwan) doped with 3-5 wt.% of PTM-3NCz in chlorobenzene was spin-coated on top of PVK layer and baked on a hot plate at 90 °C for 10 min to remove any solvent present. The samples were then transferred to a vacuum deposition system. The 60 nm-thick electron-transporting layer (ETL) (B3PYMPM), 0.8 nm-thick LiF (99.99%, Sigma-Aldrich) and 100 nm-thick aluminium were subsequently deposited by thermal evaporation under high vacuum (< $3\times10^{-6}$ mbar). The forward-viewing current–voltage–luminance characteristics of these OLED devices were measured using a Keithley 2400 source meter, Keithley 2000

multimeter and a calibrated Si photodiode (from RS components) of area 1 $cm^2$, which was placed at a distance of 2 cm from the devices. External quantum efficiencies were calculated from on-axis irradiance assuming a Lambertian emission profile and accounting for photodiode quantum efficiency across the electroluminescence spectrum. The electroluminescence spectra were obtained by a fiber spectrometer (Flame-S-VIS-NIR-ES, Ocean Optics). All the measurements were carried out at room temperature under ambient conditions.

## References


37. Körzdörfer, T.; Brédas, J.-L., Organic Electronic Materials: Recent Advances in the Dft Description of the Ground and Excited States Using Tuned Range-Separated Hybrid Functionals. *Accounts of Chemical Research* **2014**, *47*, 3284-3291.

38. Sun, H.; Hu, Z.; Zhong, C.; Chen, X.; Sun, Z.; Brédas, J.-L., Impact of Dielectric Constant on the Singlet–Triplet Gap in Thermally Activated Delayed Fluorescence Materials. *The journal of physical chemistry letters* **2017**, *8*, 2393-2398.

39. Frisch, M. J., et al., *Gaussian 09*; Gaussian, Inc.: Wallingford, CT, USA, 2009.